High-resolution near-infrared speckle interferometry and radiative transfer modeling of the OH/IR star OH 26.5+0.6

T. Driebe [1], D. Riechers [2], Y. Y. Balega [3], K.-H. Hofmann [1], A. B. Men'shchikov [4], and G. Weigelt [1]

(1) Max-Planck-Institut für Radioastronomie, Bonn, Germany

(2) Max-Planck-Institut für Astronomie, Heidelberg, Germany

(3) Special Astrophysical Observatory, Nizhnij Arkhyz, Karachaevo-Cherkesia, Russia

(4) Institute for Computational Astrophysics, Saint Mary's University, Halifax, Canada

Abstract

We present near-infrared speckle interferometry of the OH/IR star OH 26.5+0.6 in the K' band obtained with the 6m telescope of the Special Astrophysical Observatory (SAO) in Oct. 2003. At a wavelength of $\lambda = 2.12\,\mu$m the diffraction-limited resolution of 74 mas was attained. The reconstructed visibility function shows that the stellar contribution to the total flux at $\lambda = 2.12\,\mu$m is less than 50%, indicating a rather large optical depth of the circumstellar dust shell (CDS) surrounding this highly reddened object, in accordance with the strong silicate absorption feature seen in the spectral energy distribution (SED). With respect to the asymmetry found from previous observations, for instance the recent VLTI/MIDI observations in the mid-infrared (Chesneau et al. 2005, A&A 435, 563), we carefully checked our K-band data for signs of asymmetry, but given the accuracy of our measurements, no such asymmetry could be detected.

Our modeling approach follows a similar strategy as it was recently successfully applied to interpret observations of the OH/IR star OH 104.9+2.4 (Riechers et al. 2005, s. also poster at this conference). For the radiative transfer modeling of the CDS of OH 26.5+0.6 with the code DUSTY, we used our K-band vibility data from 2003 as well as various spectro-photometric data as observational input, in particular the ISO spectrum. Since OH 26.5+0.6 is a LPV, the different observations are associated with different phases of the object's variability cycle. For instance, while the ISO observations were carried out close to minimum phase (ϕ=0.5), our K-band visibility data correspond to ϕ=0.13. From our analysis, we derived several physical parameters of the central star and the CDS as as function of pulsation phase.

Introduction

The vast majority of OH/IR stars are long-period variables (pulsation periods between 500 and ∼2000 d) of variability type Me, similar to long-period Mira stars, exhibiting strong OH maser emission at either 1612 or 1665/1667 Mhz. While nearly all OH/IR stars show a bolometric amplitude of typically $\sim 1^{\rm m}$, a very small fraction varies irregularly with a low amplitude or does not show any detectable variability. OH/IR stars are mostly low and intermediate mass (progenitor masses $M \leq 9\,M_\odot$), oxygen-rich single stars evolving along the upper part of the asymptotic giant branch (AGB). As a consequence of their high mass loss (up to several $10^{-4} M_\odot$/yr), OH/IR stars are usually surrounded by massive, optically and geometrically thick circumstellar envelopes composed of gas and dust. The strong maser emission reveals in nearly all cases a non-rotating CDS, which, in some cases, totally obscures the underlying star. In the common picture of stellar evolution, OH/IR stars are believed to represent an object class following the classical Mira star stage at the very end of the AGB star, which makes them ideal targets to investigate where the transition from the ususally spherical CDS of AGB stars to the mostly axis-symmetric planetary nebulae takes place.

OH 26.5+0.6 is a well-studied and, in many respects, an outstanding example for highly evolved and highly dust-enshrouded OH/IR stars. It is one of the brightest OH maser sources, and with $F_{12\mu m} \approx 360$ Jy this object is among the 100 brightest southern IRAS points sources. OH 26.5+0.6 is a long period variable with a period of $P = 1559 \pm 6.6$ d (Suh & Kim 2002, our study) located at a distance of 1.37 kpc (van Langevelde et al. 1990).

Observations

We obtained K-band visibilities of OH 26.5+0.6 from speckle-interferometric observations with the 6 m telescope of the Special Astrophysical Observatory (SAO) in Russia on October 15, 2003 The data were recorded with our HAWAII speckle camera through interference filters with a center wavelength of 2.125 μm and a bandwidth of 0.214 μm (K_s filter). The visibility function of OH 26.5+0.6, i.e. the modulus of the Fourier transform of its intensity distribution, was derived from the speckle interferograms using the speckle interferometry method (Labeyrie 1970).

The reconstructed two-dimensional visibility of OH 26.5+0.6 at 2.125 μm and the visibility profile azimuthally averaged over all angles are shown in Figs. 1a and c, respectively. As Fig. 1c reveals, the azimuthally averaged visibility decreases steadily to values below ∼ 0.35 at spatial frequencies of 10 cycles/arcsec Thus, the CDS is almost fully resolved, and the contribution of the unresolved component to the monochromatic flux at $\lambda = 2.125\,\mu$m is less than ∼ 35 %, indicating a rather large optical depth at this wavelength.

Stimulated by the ongoing debate about the possible asymmetry of the CDS of OH 26.5+0.6 (see Chesneau et al. 2005 for a discussion), we carefully checked our data for such asymmetries. We looked for possible intrinsic asymmetries by comparing radial cuts of the 2D visibility calculated from an average over 4 different position angle segments, each covering 45°, as indicated in Fig. 1a. The resulting visibility cuts are displayed in Fig. 1b. In this figure, for the sake of clarity error bars are shown only for one of the four curves. As the figure illustrates, within the error bars there is very good agreement among all 4 averaged visibility curves. Therefore, given the accuracy and resolution of our visibility measurement, we conclude that in the K band the CDS of OH 26.5+0.6 appears spherically symmetric in accordance with OH maser maps. Based on our data, the K-band diameter ratio between major and minor axis deviates from unity by less than 2 %.

From an analysis of K-band spectro-photometric data we found a pulsation period of 1560 d for OH 26.5+0.6 in accordance with Suh & Kim (2002). From our lightcurve fit (see Fig. 2), we derived a phase $\Phi_{\rm SAO} = 0.13$ for our K-band observation.

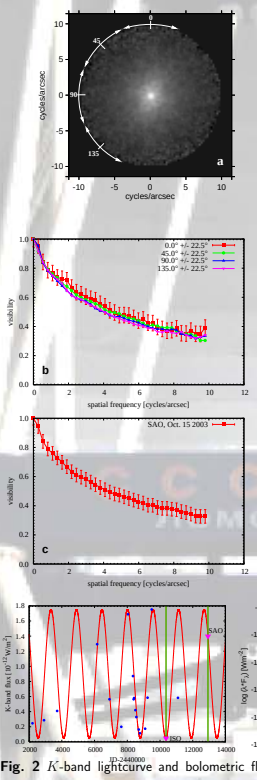

Fig. 1: Observations of OH 26.5+0.6 on October 15, 2003, with the SAO 6 m telescope. **a**: 2-dimensional visibility function of OH 26.5+0.6 in the K band at 2.125 μm. North is up and east is to the left. **b**: Azimuthally averaged visibility of OH 26.5+0.6 in the K band obtained from the 2D visibility shown in panel a. The four curves are the visibilities azimuthally averaged between position angles -180° and -135° (solid line), between -135° and -90° (dashed), between -90° and -45° (dotted), and between -45° and 0° (dash-dotted), respectively. For clarification, only for one of the curves representative error bars are shown. The figure illustrates that there is a marginal asymmetry towards a position angle close to 0°, but given the accuracy an asymmetry of the CDS of OH 26.5+0.6 can not be concluded from the measurements presented here. **c**: Azimuthally averaged visibility of OH 26.5+0.6 in the K band obtained from the 2D visibility shown in panel a. The visibility shown here was derived from an azimuthal average over all position angles.

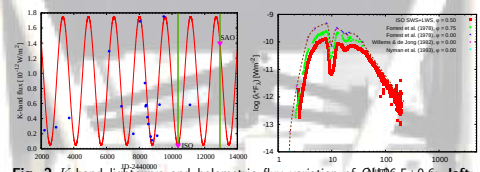

Fig. 2 K-band lightcurve and bolometric flux variation of OH 26.5+0.6: **left**: Recent spectro-photometric observations at $\lambda = 2.2\,\mu$m. The filled bullets indicate measurements by different authors (see Driebe et al. 2005 for references). A 4-parameter cosine function is fitted to the data, giving a pulsation period of $P = 1560 \pm 20$ d in very good agreement with the result from Suh & Kim (2002). The left vertical dashed line indicates the date of the ISO measurements and substantiates the assumption of $\Phi_{\rm ISO} = 0.5$. The right vertical dashed line indicates the date of the SAO measurements. From the lightcurve fit we find $\Phi_{\rm SAO} \simeq 0.13$. **right:** IR variability of OH 26.5+0.6: The figure shows the ISO SWS+LWS spectra as well as other spectro-photometric data (see labels, for references see Driebe et al. 2005) According to the lightcurve fit shown in panel a, the ISO spectra can be associated with minimum pulsation phase, while most of the data from Forrest et al. correspond to an intermediate (bullets) phase, and the second data set from Forrest et al. (1978) as well as the data from Willems & de Jong (1982), and Nyman et al. (1993) correspond to maximum phase. Using these data a maximum phase, we constructed a maximum envelope (dashed line), from which we derived $F_{\rm bol}^{\rm max} = 7.15 \pm 0.35 \cdot 10^{-10}\,{\rm W/m^2} \approx 4 \cdot {\rm F}_{\rm bol}^{\rm ISO} = {\rm F}_{\rm bol}^{\rm min} = 1.78 \pm 0.10 \cdot 10^{-10}\,{\rm W/m^2}$.

Radiative Transfer Modeling

We used the 1-D radiative transfer code DUSTY (Ivezic & Elitzur 1997) to simultaneously model the K-band visibility and the SED of OH 26.5+0.6 measured at different epochs to determine the temporal change of some physical parameters of the CDS. The results for our final quasi-time-dependent radiative transfer model are visualized and summarized in Fig. 3 and Tab. 1, respectively. As the lower panels in Fig. 3 illustrate, our final model is able to fairly reproduce the SED for different phases as well as our K-band visibility measurement. In this model, the dust density profile has been calculated from a radiatively driven wind approach. No superwind phase had to be assumed to find a good match with the observations. The optical properties of the silicate dust grains have been taken from Suh (1999), and the grain size distribution follows the description of Mathis, Rumpl & Nordsieck (1977) with a power index of 3.5.

According to our final model, the bolometric flux of OH 26.5+0.6 varies by ∼ a factor of 4 between minimum and maximum phase. Due to its variability the temperature of the central source increases by ∼ 1000 K from minimum to maximum phase while the stellar radius decreases by $\sim 100 R_\odot$. Correspondingly, the inner dust shell boundary moves by a factor of ∼ 2.4. optical depth in the 10 μm regime drops by a factor of ∼ 2. Thus, our results are similar to our findings for another OH/IR source, OH 104.9+2.4 (Riechers et al. 2005, see also poster by Riechers et al.).

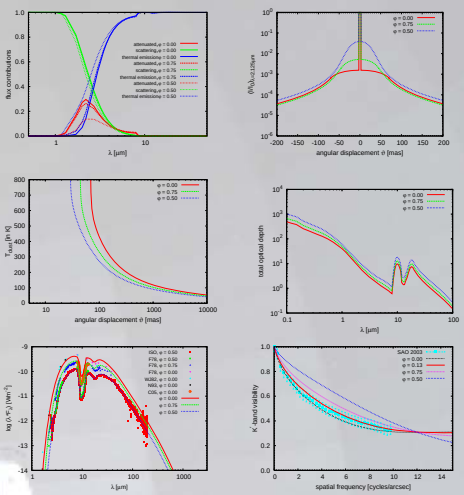

Figure 3: Variation of the dust shell properties of OH 26.5+0.6 as a function of pulsation phase (see Tab. 1). **Top left**: Fractional contributions to the total flux. The contribution from direct stellar light is small compared to the contribution of dust scattering and thermal emission. **Top right**: The normalized intensity profile at 2.125 μm. The sharp central peak corresponds to the central source of radiation. **Middle left**: Dust temperature as a function of angular distance. The point where $T_{\rm dust} = 800$ K indicates the inner radius of the dust shell. As the figure shows, due to the variability of the central source the inner dust shell boundary moves from 29.3 mas (= 10.1 R_*) to 69.5 mas (= 27.0 R_*) between minimum and maximum pulsation phase. **Middle right**: Wavelength dependence of the total optical depth. **Bottom left**: Spectral energy distribution. **Bottom right**: K-band visibility. Our 2003 measurement (filled squares) is shown for comparison with the model for phase $\Phi_{\rm SAO} = 0.13$.

Parameter	unit	$\Phi = 0.0$	$\Phi = 0.13$ SAO (2003)	$\Phi = 0.25$	$\Phi = 0.5$ ISO
Temperature at inner CDS boundary*	[K]	800	800	800	800
Minimum grain size*	[μm]	0.005	0.005	0.005	0.005
Maximum grain size	[μm]	0.30	0.295	0.28	0.25
Gas-to-dust ratio*		200	200	200	200
Optical depth					
$\lambda = 0.55\,\mu$m		100	110	130	180
$\lambda = 2.2\,\mu$m		6.1	6.6	7.5	9.9
$\lambda = 9.7\,\mu$m		9.4	10.3	12.3	17.8
Central star luminosity	[$10^4\,L_\odot$]	4.17	3.09	2.04	1.04
Central star effective temperature	[K]	3000	2800	2500	2000
Central star radius	[$R_\odot$]	758	749	764	852
	[mas]	2.58	2.55	2.59	2.89
	[AU]	3.5	3.5	3.6	4.0
Radius of inner CDS boundary	[R_*]	27.0	22.8	17.2	10.1
	[mas]	69.5	58.0	44.6	29.3
	[AU]	95.2	79.5	61.1	40.1
Mass-loss rate	[$10^{-5}\,M_\odot$/yr]	12.1	9.3	6.4	2.9
Bolometric flux	[$10^{-10}\,{\rm W/m^2}$]	7.15	5.30	3.50	1.78

Tab. 1: Parameters of the dust shell and central star of OH 26.5+0.6 at different pulsation phases according to our final radiative transfer model. Quantities marked with * have been kept fixed in the simulations.

References

- Chesneau, O., Verhoelst, T., Lopez, B., et al. 2005, *A&A* **435**, 563
- Driebe, T., Hofmann, K.-H., Ohnaka, K., et al. 2005, *A&A* , submitted
- Labeyrie, A. 1970, *A&A* **6**, 85
- Ivezic, Z., Elitzur, M. 1997, *MNRAS* **287**, 799
- Mathis, J. S., Rumpl, W., Nordsieck, K.H. 1977, *ApJ* **217**, 425
- Suh, K.-W. 1999, *MNRAS* **304**, 389
- Suh, K.-W., Kim, H.-Y. 2002, *A&A* **391**, 665
- Riechers, D., Balega, Y.Y., Driebe, T., et al. 2005, *A&A* **436**, 925
- van Langevelde, H. J., van der Heiden, R., & van Schoonefeld, C. 1990, *A&A* **239**, 193

Poster presented at the Annual Scientific Meeting of the Astronomische Gesellschaft

The many facets of the universe - Revelations by new instruments

26th Sept. – 1st Oct. 2005, Cologne, Germany

contact e-mail: driebe@mpifr-bonn.mpg.de